MST Radar Observations of Gravity Waves and Turbulence near Thunderstorms

ANTHONY R. HANSEN, GREGORY D. NASTROM, AND JASON A. OTKIN*

Department of Earth Sciences, St. Cloud State University, St. Cloud, Minnesota

FRANK D. EATON

Air Force Research Laboratory, Kirtland Air Force Base, New Mexico

(Manuscript received 15 March 2001, in final form 25 June 2001)

ABSTRACT

The effect of deep convection on the intensities of gravity waves and turbulence during the summer at White Sands, New Mexico, is investigated using 50-MHz mesosphere–stratosphere–troposphere (MST) radar observations and surface weather reports. Radar data taken at 3-min intervals from the summers of 1991 through 1996 (with occasional gaps of varying length) are used to construct hourly means, medians, and standard deviations of wind speed, spectral width (σ^2_{turb}), and backscattered power calibrated as the refractivity turbulence structure constant (C_n^2). The hourly variance of the vertical velocity σ_w^2 is used as an indicator of high-frequency gravity wave intensity. Surface observations taken near the radar site are used to identify periods marked by convection at or near the radar. During cases in which no convection is reported, the median hourly σ_w^2 is nearly constant with altitude (about 0.04 $\text{m}^2\ \text{s}^{-2}$ below and 0.03 $\text{m}^2\ \text{s}^{-2}$ above the tropopause). Values of σ_w^2, C_n^2, and σ^2_{turb} are significantly enhanced from no-convection cases to thunderstorm cases. Largest increases are about 12 dB relative to the no-convection cases at about 11 km for σ_w^2, about 9.5 km for σ^2_{turb}, and about 7.5 km for C_n^2. The relatively lower height for the maximum of C_n^2 is likely due to the influence of humidity advected upward during convection on the mean gradient of the refractive index. The probability density distributions of C_n^2 and σ^2_{turb} near their levels of maximum enhancement are unimodal, with the modes steadily increasing with increasing proximity of convection. However, the probability density distribution of σ_w^2 is bimodal in all instances, suggesting that there can be enhanced wave activity even when visible convection is not present and that the presence of a thunderstorm at the station does not necessarily indicate greatly enhanced wave activity.

1. Introduction

Deep convection has long been recognized as a major source both of gravity waves and turbulence (e.g., Gossard and Hooke 1975). The intermittent nature of convection in both space and time makes observational studies challenging, but the high spatial and temporal resolution of mesosphere–stratosphere–troposphere (MST) radars offers a useful tool for measuring the effects of convection on the generation of waves and turbulence (Gage 1990). Case study results (over a few hours to a few days) of MST radar observations from several sites around the world show enhanced gravity wave activity during convective events (e.g., Roettger 1980; Ecklund et al. 1981; Larsen et al. 1982; Lu et al. 1984; Bowhill and Gnanalingam 1986; Sato 1992, 1993; Sato et al. 1995; Petitdidier et al. 1997; Rüster et al. 1998). Also, climatological studies of the standard deviations of vertical velocity about hourly means (taken as an indicator of gravity wave intensity) from MST radar observations show diurnal patterns with afternoon maxima that have been qualitatively attributed to convective activity (e.g., Nastrom and Gage 1984; Nastrom and Eaton 1995). Other measurement platforms also show convection as a major source of gravity waves, including balloons (Tsuda et al. 1994; Vincent and Alexander 2000), aircraft (Fritts and Nastrom 1992), and satellites (Dewan et al. 1998; McLandress et al. 2000), although these observations generally have poorer resolution in time or in the vertical than MST radar observations. Numerical modeling work has examined the generation of waves by thunderstorms (e.g., Alexander et al. 1995; Yang and Houze 1995; Pandya and Alexander 1999; Lane et al. 2001; Lane and Reeder 2001), and the effects of such waves on the general circulation (e.g., Chun et al. 2001).

Recently, Hansen et al. (2001) found a significant peak during summer in the energy density of short-period (6 min to 2 h) waves in the upper troposphere

* Current affiliation: Department of Atmospheric and Oceanic Sciences, University of Wisconsin—Madison, Madison, Wisconsin.

Corresponding author address: Dr. Anthony R. Hansen, Department of Earth Sciences, St. Cloud State University, 720 Fourth Avenue South, St. Cloud, MN 56301-4498.
E-mail: ahansen@stcloudstate.edu

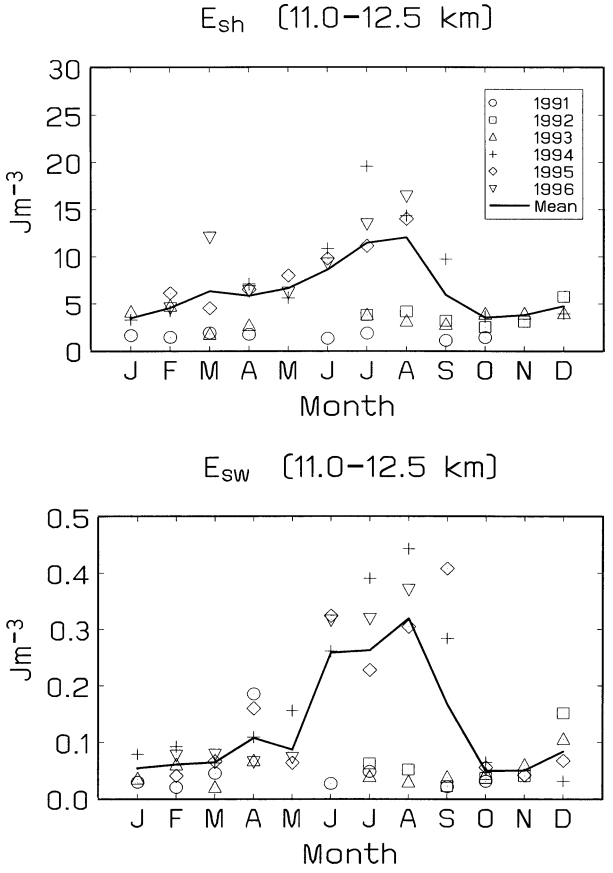

FIG. 1. Composite mean seasonal cycle of the kinetic energy density of high-frequency gravity waves for (top) horizontal E_{sh} and (bottom) vertical E_{sw} motions at 11.0–12.5 km at WS. Individual monthly values are also plotted as symbols (see legend) (Hansen et al. 2001).

both in the horizontal (E_{sh}) and vertical (E_{sw}) motions from MST radar observations at White Sands, New Mexico (WS). They tentatively suggested the peak might arise from waves launched by deep convection associated with the summer monsoon in the southwestern United States. Indeed, comparison of the monthly march of E_{sh} and E_{sw} (Fig. 1) with that of thunderstorm reports at El Paso (ELP; Fig. 2a), located about 50 km from WS, supports this suggestion. However, this casual agreement is very general. The goal of the present study is to perform more detailed comparisons. For example, since convection is highly intermittent it seems likely that wave intensity will depend upon the distance (in space or time) between the convection and the radar. In order to explore this suggestion, we will compare the radar observations with surface observations of convection made at the weather station located only a few kilometers from the radar.

Convection also causes increased turbulence. Past case studies of backscattered power (e.g., Green et al. 1978) and eddy dissipation rate (Sato et al. 1995) report increased turbulence due to convection. The diurnal patterns of the refractivity turbulence structure constant

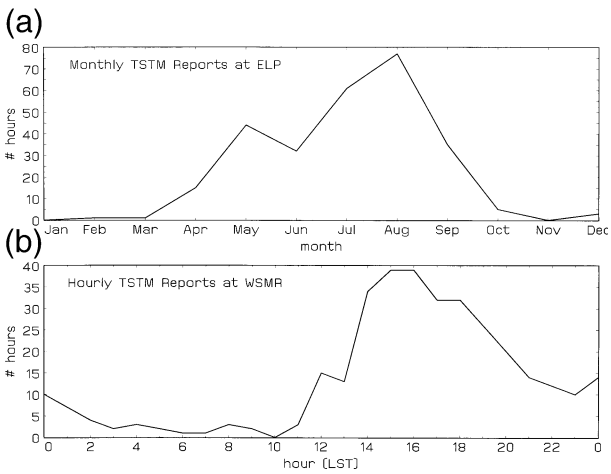

FIG. 2. (a) Frequency distribution of the number of thunderstorm reports at ELP as a function of calendar month (1991–96), and (b) frequency distribution of the number of thunderstorm reports at the weather station at WS as a function of LST during the months of Jul and Aug (1991–92).

C_n^2 [which is related to the backscattered power (Gage 1990)] and of the Doppler spectral width given by Nastrom and Eaton (1995) both show afternoon summer maxima, which they suggest are due to the effects of convective activity. The amplitudes of the turbulence variables as functions of distance from the convection are also included in the present study in order to explore this suggestion.

The paper is organized as follows. The data from WS are discussed in section 2. Median profiles and frequency distributions of wave and turbulence indicators, sorted according to the proximity of thunderstorms, are given in section 3. Summary comments and conclusions are contained in section 4.

2. Data

The data used in the present study were obtained from the 50-MHz radar located at the White Sands Missile Range (32°24′N, 106°21′W, 1220 m above sea level). The WS radar is located in locally flat terrain between two relatively high north–south-oriented mountain ranges (Nastrom and Eaton 1995). These mountains are known sources of topographically forced gravity waves during high wind conditions (Nastrom and Eaton 1993, 1995). Observations were made using Doppler spectra on three beams: vertical and 15° from the zenith in the north–south and east–west planes. The radar system observes along each beam for ~1 min and cycles through a complete profile approximately every 3 min. The 3-min data were used to produce hourly means, medians, and standard deviations of wind speed, spectral width, and C_n^2. In this study, the variance of the vertical wind speed about its hourly mean is assumed proportional to the energy in short-period (6–60 min) gravity waves. Thus we are sampling only a part of the short-period

wave spectrum. Here, C_n^2 and spectral width are assumed related to the intensity of turbulence on length scales in the inertial subrange (Gage 1990). Following Nastrom and Eaton (1997), the corrected spectral width (σ_{turb}^2) is given by $\sigma_{\text{turb}}^2 = \sigma_{\text{obs}}^2 - \sigma_{\text{corr}}^2$, where σ_{obs}^2 is the observed spectral width and σ_{corr}^2 is the sum of the corrections for beam-, shear- and wave-broadening effects. Useful data were obtained on the oblique beams from ~5–20-km altitude and on the vertical beam from ~7–20 km with a nominal vertical spacing of 150 m. The lower limits are determined by radar electronics systems and the upper limit from signal-to-noise thresholds [see Nastrom and Eaton (1993) for further technical details on the radar]. The WS radar data span the period from January 1991 through September 1996, with occasional gaps of varying length.

Surface hourly observations taken at the weather station (called C Station) located approximately 4 km south of the radar were used to identify periods marked by convection at or near the radar. These hourly observations included routine meteorological data as well as extensive remarks on clouds (including shallow cumulus and towering cumulus) and thunderstorms at or in the vicinity of WS. Weather reports from C Station were available on a 24 h day^{-1} basis during 1991–92, from 0400 to 1900 LST during 1993–94, and from 0700 to 1600 LST during 1995–96.

3. Results

Figure 1 shows that the mean E_{sh} and E_{sw} are largest in June through August when they increase by factors of 3–6 above the winter values [although interannual variability is large as discussed in Nastrom and Eaton (1997) and Hansen et al. (2001)]. During these summer months the mean winds at WS from the midtroposphere through the lower stratosphere are less than 10 m s^{-1} at all altitudes (Hansen et al. 2001). Thus, sources of gravity waves related to winds, such as flow over topography or shear induced waves, are unlikely to explain the strongly enhanced kinetic energy densities.

In an effort to quantify the impact of deep convection on the intensity of high frequency gravity waves and turbulence, the WS radar data during June through September were sorted based upon four possible criteria. One group was formed for all hours in which no convection was present at C Station. Hours with any convective clouds (e.g., cumulus, towering cumulus, altocumulus castellanus, cirrocumulus) were excluded from this group. Three other groups were formed for hours in which convection was reported as: 1) distant from the site; 2) nearby, but not at C Station; and 3) when thunderstorms were reported at C Station (i.e., the weather observer could hear thunder, although a thunderstorm was not necessarily directly over the weather station). Median profiles were formed for each group for the hourly variance of the vertical velocity σ_w^2 (an indicator of high-frequency gravity wave intensity), log C_n^2 (a measure of the intensity of refractivity turbulence), σ_{turb}^2 (an indicator of mechanical turbulence closely related to the kinetic energy dissipation rate), and the hourly median zonal wind speed (in order to crudely characterize the large-scale flow). Fig. 2b shows that the probability of thunderstorms at WS for the months of July and August 1991–92 has a strong diurnal cycle with values increasing quickly from around 1200 LST to a peak at 1500–1600 LST before tapering off in the evening.

Figure 3 shows the median profiles for the four convection groups for all hours of the day. The median σ_w^2 profiles (Fig. 3a) reveal that for the no-convection group the vertical velocity fluctuations are modest and uniform from 7- to 20-km altitude. (A slight discontinuity occurs at the tropopause, about 15 km, with σ_w^2 decreasing from about 0.04 m^2 s^{-2} below to about 0.03 m^2 s^{-2} above; presumably because there is increased static stability in the stratosphere and waves conserve energy). Increasingly larger values of σ_w^2 are found when convection is present and progressively nearer the station. For distant convection there is a roughly 100% increase in σ_w^2 from 7 to 12 km with smaller increases at higher altitudes compared to no-convection hours. Cases of nearby convection show about a fourfold increase in σ_w^2 at 7–12 km. The largest increases compared to no-convection hours occur when a thunderstorm is observed at C Station. At about 10–12 km the increase is about a factor of 15. Above the tropopause from 16 to 20 km, σ_w^2 increases by roughly a factor of 3 when thunderstorms are observed at the station compared to no-convection hours. Error bars that correspond to $\pm\sigma(N_0)^{-1/2}$ (where σ is the standard deviation of the N_0 values used) are given for the no-convection and the thunderstorm profiles.

The present results can be compared to other observational studies. Lu et al. (1984) observed an enhancement of vertical velocity variance measured by MST radar in the presence of thunderstorms in eastern Colorado during subsets of a 12-day observing period. They found increases in σ_w^2 up to a factor of 4–4.5 at altitudes from 8.1 to 10.5 km. This compares to a factor of 5 enhancement through a deeper layer (7–13 km) in the ''nearby'' thunderstorm group in the present case (which may be the most comparable subset of the present data to Lu et al.'s result). In addition, Sato (1993) found vertical velocity variances averaging roughly 0.3 m^2 s^{-2} for wave periods less than an hour in the 9–16-km layer in the presence of deep convection near the middle and upper atmosphere (MU) radar in Japan during the passage of Typhoon Kelly. This compares to an average of 0.4 m^2 s^{-2} in the same layer in the present thunderstorm sample. After the typhoon passed, Sato (1993) found roughly 0.13 m^2 s^{-2} variance in the same layer when deep convection was not near the radar site. This value lies between the present nearby and ''distant'' convection groups, which may be representative of the conditions reported in Sato (1993).

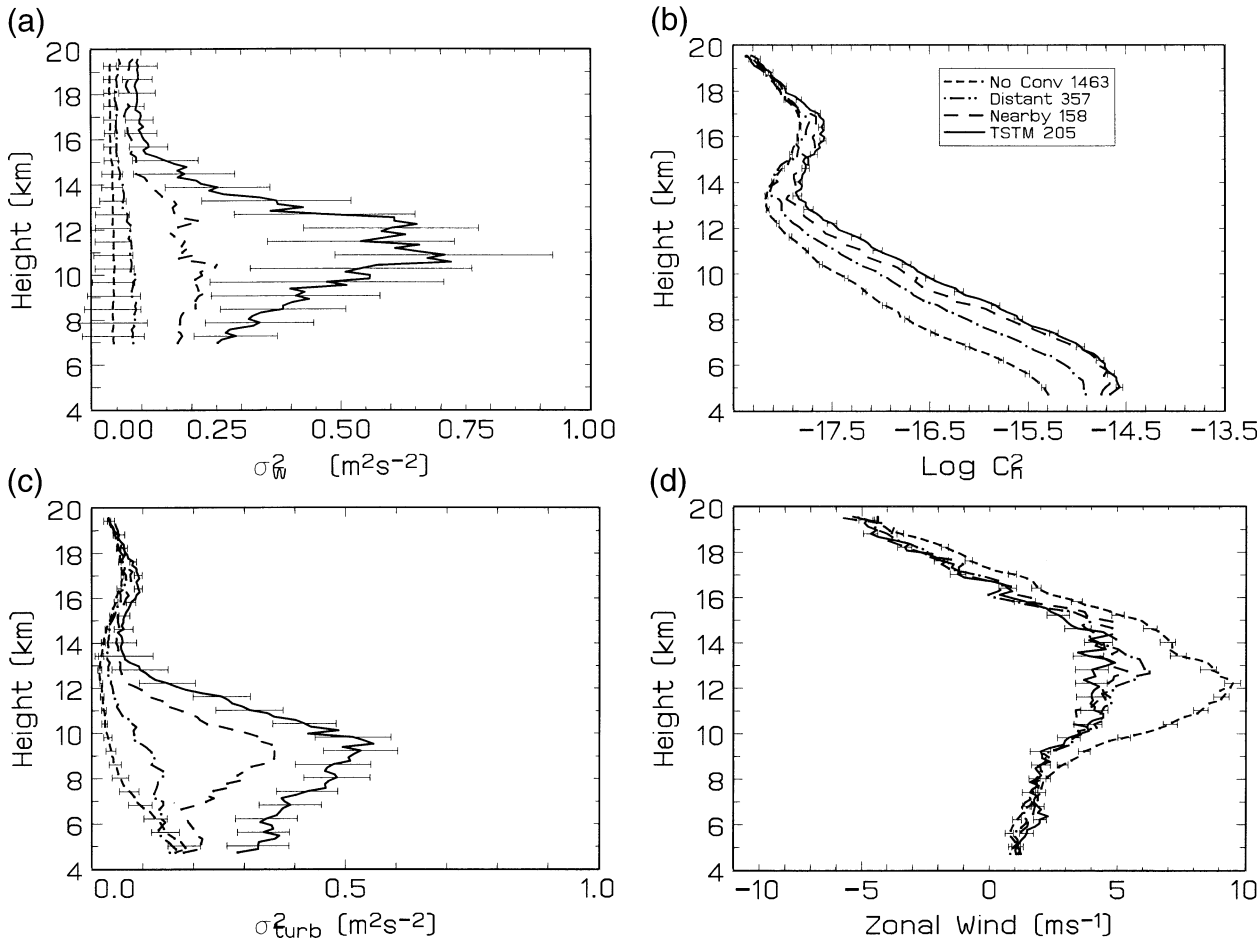

FIG. 3. Composite median profiles of (a) σ_w^2, (b) log C_n^2, (c) σ_{turb}^2, and (d) zonal wind speed for hours with no convection (short-dashed line), convection observed distant from the weather observing site (dot-dashed line), convection nearby (long-dashed line), and thunderstorms observed at the site (solid line). The error bars on the figure represent estimates of the standard errors in the medians; the numbers for each sample given in the legend indicate the number of hourly values used.

In addition, the present results in the upper troposphere are reminiscent of the dramatic increase in vertical velocity variance in the upper troposphere in the squall line simulation of Alexander et al. (1995). Yang and Houze (1995) attribute similar features in their squall line simulation to vertically trapped gravity waves. Alexander et al. (1995) also illustrate gravity-wave-induced vertical velocity variance in the lower stratosphere above their simulated thunderstorm, which may correspond to the enhanced σ_w^2 in the lower stratosphere for our cases of nearby convection and convection observed at the station. Recent modeling studies by Lane et al. (2001) and Lane and Reeder (2001) illustrate convectively generated gravity waves trapped in the troposphere as well as waves propagating vertically in the lower stratosphere from simulated thunderstorms developing in both a relatively weakly sheared environment and a more strongly sheared environment. The inferred vertical velocity variances in such simulations may be analogous to the results in the middle to upper troposphere and lower stratosphere of the present observational study.

Figure 3b shows the profiles of log C_n^2 for the four groups. The C_n^2 profiles indicate a progressive increase in the intensity of refractivity turbulence with the proximity of thunderstorms. The largest differences occur in the middle to upper troposphere. The value of C_n^2 is proportional to the product of the outer scale of turbulence and the mean gradient of the refractive index (Gage 1990). Since the mean gradient of the refractive index depends strongly upon humidity, the changes seen at tropospheric levels in Fig. 3b are strongly influenced by the increased water vapor in the vicinity of the thunderstorms. The C_n^2 differences taper off with altitude and the curves are approximately the same for convective and nonconvective samples above 18-km altitude.

Figure 3c shows the median curves of σ_{turb}^2 for the four groups. Assuming that the atmosphere is stably stratified, σ_{turb}^2 is related to the eddy dissipation rate (ε) as $\varepsilon = AN\sigma_{\text{turb}}^2$, where A is a constant and N is the Brunt–

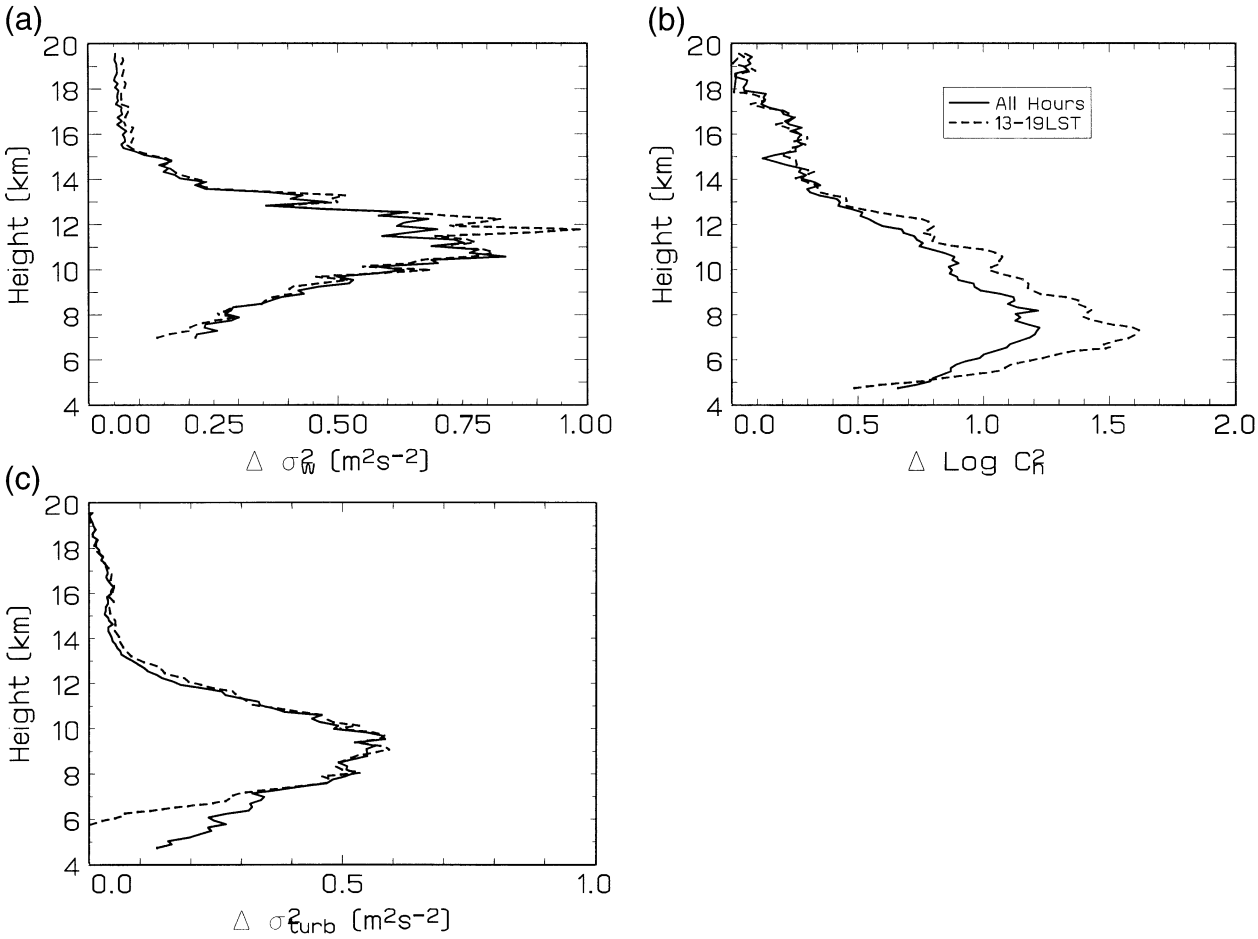

FIG. 4. Comparison of the differences between the profiles of (a) σ_w, (b) log C_n^2, and (c) σ_{turb}^2 for hours with thunderstorms reported and hours with no convection present for all hours of the day (solid line) and only hours between 1300 and 1900 LST (the peak hours of convection during the summer; dashed line).

Väisälä frequency (Weinstock 1981). The results show progressively larger values of σ_{turb}^2 in the midtroposphere with the increasing proximity of convection. At about 9–10 km there is more than a tenfold increase for the thunderstorm group compared to the no-convection group. (It is interesting that the wave broadening corrections in σ_{turb}^2 were found to be small in all four groups despite the large changes in σ_w^2.)

Profiles of the background flow are also given (Fig. 3d). The groups, when convection is present, all have very weak background winds, generally less than 5 m s^{-1} throughout the troposphere and small associated vertical shear. In contrast, the no-convection group shows a stronger vertical wind shear in the troposphere (in Fig. 3d, the shear is 7 m s^{-1} between 8 and 12 km). If only July and August cases are considered, the mean upper tropospheric winds are similar for all groups, but the no convection group winds show a 4 m s^{-1} shear from 4 to 10 km, whereas all of the convection cases exhibit approximately zero shear in this layer. This pattern suggests that stronger vertical wind shear may inhibit deep convection in the vicinity of WS. The results in Fig. 3d further confirm that mechanisms related to wind shear or flow over topography are unlikely to explain the strong waves and turbulence observed in the presence of deep convection.

The no-convection group in Fig. 3 includes observations from both day and night while the convection groups are weighted toward afternoon because most thunderstorms occur in the afternoon. Since there may be changes in waves or turbulence induced by diurnal effects not associated with thunderstorms, it might be suggested that the differences seen in Fig. 3 are due to diurnal rather than convective effects. In an effort to test this suggestion the differences between the profiles for all nonconvection hours and for all hours with thunderstorms at C Station (as in Fig. 3) are contrasted in Fig. 4 with differences formed from only the hours 1300–1900 LST, which are the hours of peak convective activity at WS (Fig. 2b). Figure 4 shows the changes between profiles of no-convection and thunderstorms are nearly identical regardless of time of day, indicating

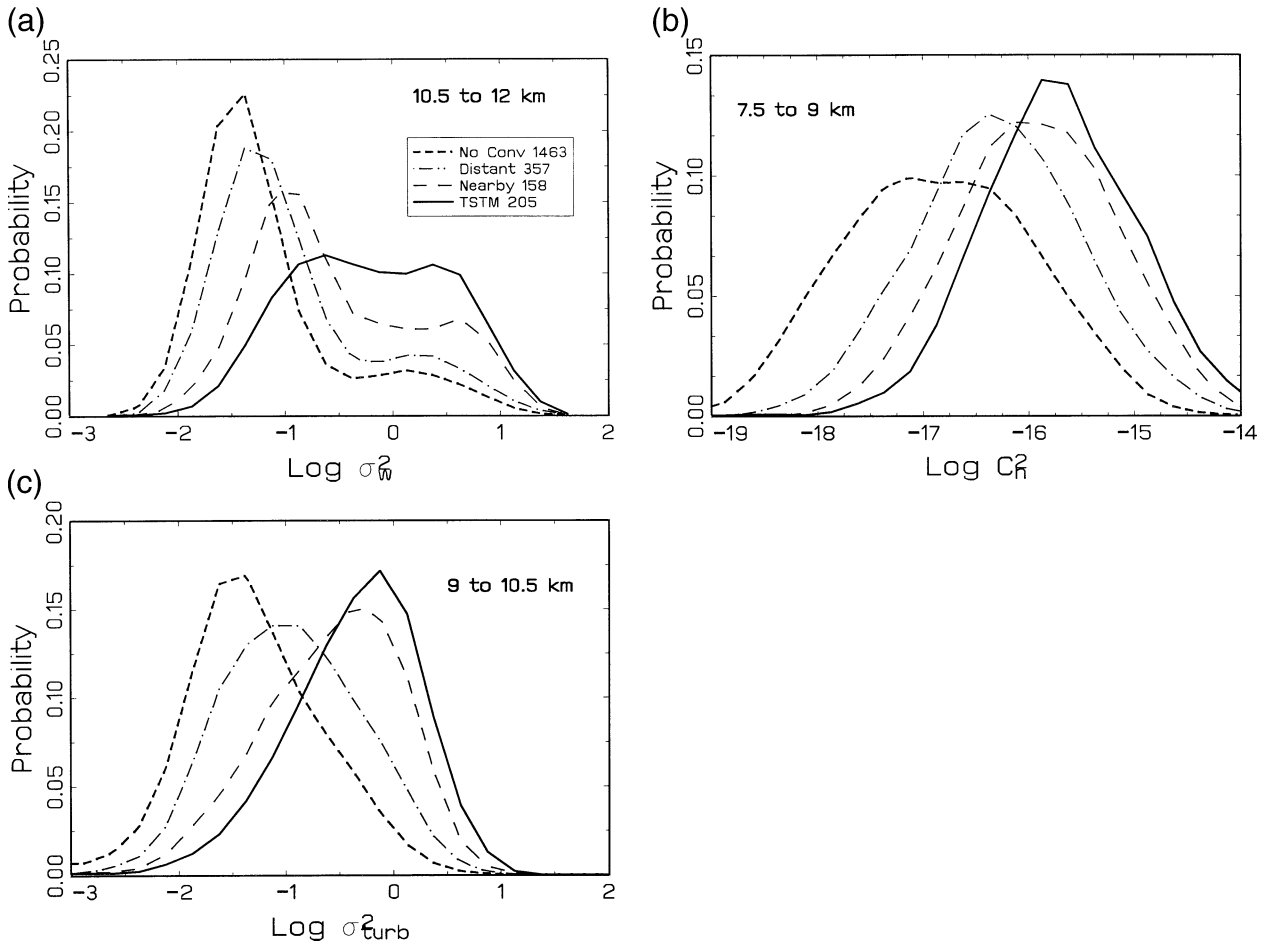

FIG. 5. Probability density distributions for observations through a 1.5-km layer near the level of maximum enhancement of the thunderstorm group relative to the no-convection group for each variable (altitudes as indicated on each figure). The distributions were computed as smoothed histograms (Rosenblatt 1956) with a class interval of 0.25 in each case.

that the results in Fig. 3 are not an artifact of a climatological diurnal change. In Fig. 4, 334 (169) profiles are used for the no-convection (thunderstorm) cases.

In Fig. 4, the maximum enhancement of σ_w^2 (about 0.75 $m^2\ s^{-2}$; i.e., about 12 dB relative to the no-convection profile) during thunderstorms is found at about 11 km. This is near the top of typical thunderstorms at WS and thus near the level of maximum generation of waves by penetrative convection (Gossard and Hooke 1975; Roettger 1980). The maximum enhancement during thunderstorms of σ_{turb}^2 is found slightly lower, at about 9.5 km, slightly below typical thunderstorm tops. The magnitude of the maximum enhancement of σ_{turb}^2 is about 0.55 $m^2\ s^{-2}$ (about 12 dB) relative to the no-convection profile. The maximum enhancement of log C_n^2 is at lower altitude, at about 7.5 km. Its magnitude is about 12 dB for all hours (over 15 dB when only afternoon hours are compared), and probably results from the combined effects of enhanced mechanical turbulence associated with convection and the enhanced mean gradient of the refractive index due to upward moisture flux in convection.

It is of interest to examine the probability density distributions of these variables. Figure 5 shows the probability density distributions of observations in a 1.5-km layer near the level of maximum enhancement for each data group for each variable (10.5–12 km for σ_w^2, 9–10.5 km for σ_{turb}^2, and 7.5–9 km for C_n^2). The distributions for log σ_w^2 have two modes for each of the groups, a high-energy mode near 0.5 and a low-energy mode that migrates from about -1.4 for the no-convection group to about -0.6 for the thunderstorm group. Apparently, during some thunderstorms the gravity waves produced propagate directly over the radar whereas during other thunderstorms they do not.

The existence of the high-energy mode in the no-convection cases might be understood in terms of the structure of the wind field. In an effort to explore this possibility, Table 1 shows the mean zonal winds (u) at 5.6 and 12 km for cases of small and large log σ_w^2 for

TABLE 1. Mean zonal wind speed u for no-convection and thunderstorm groups for cases of low and high σ_w^2. Error bounds indicate $\pm 2\sigma(N_0)^{-1/2}$.

	No-convection hours		Thunderstorm hours	
	$\log \sigma_w^2 < -1$	$\log \sigma_w^2 > -0.32$	$\log \sigma_w^2 < -0.32$	$\log \sigma_w^2 > 0$
N_0	909	261	78	92
u (5.6 km)	0.7 ± 0.4	0.2 ± 0.6	0.9 ± 1.1	1.9 ± 0.6
u (12 km)	10.8 ± 0.8	5.6 ± 1.4	4.9 ± 2.0	5.5 ± 1.7

the no-convection cases and for the thunderstorm cases. Note that for the thunderstorm cases u is about the same for small and large $\log \sigma_w^2$. For the no-convection cases, winds are weak at 5.6 km for both large and small $\log \sigma_w^2$. This pattern argues against a topographic source for the high variance in the latter case. However, the winds at 12 km are significantly smaller for the large $\log \sigma_w^2$ group, suggesting that summertime gravity wave activity is enhanced in the absence of deep convection during light winds aloft. Perhaps waves launched by convection at the top of the planetary boundary layer (but not accompanied by visible clouds) are more likely to propagate to the upper troposphere during light wind conditions. It is well known that critical-level filtering depends strongly on the mean wind profile [e.g., see the recent review by Whiteway (1999)].

In Fig. 5 the probability density distributions for $\log C_n^2$ and $\log \sigma_{\text{turb}}^2$ have a single mode for each data group. The modes migrate toward larger values going from the no-convection to the thunderstorm groups. The distributions for $\log C_n^2$ appear normal, consistent with past studies (e.g., Nastrom and Eaton 1995). However, the distribution for $\log \sigma_{\text{turb}}^2$ is not symmetric about the mode, but rather is slightly positively skewed for the no-convection curve and slightly negatively skewed for the thunderstorm curve. Explanation of this skewness is left to future study.

4. Summary and conclusions

The effect of convection on the intensities of gravity waves and turbulence during the summer at WS has been investigated using 50-MHz radar observations and surface weather reports. The following conclusions have been reached:

1) The maximum frequency of thunderstorms at WS during June through September is in the afternoon, at 1300–1900 LST.
2) During cases when no convection is reported, the median hourly σ_w^2, an indicator of gravity wave intensity, is nearly constant with altitude (about 0.04 $\text{m}^2\,\text{s}^{-2}$ below and 0.03 $\text{m}^2\,\text{s}^{-2}$ above the tropopause).
3) The values of σ_w^2, C_n^2, and σ_{turb}^2 are significantly enhanced from no-convection cases to thunderstorm cases. The largest increases are about 12 dB relative to the no-convection cases. The largest increases are at about 11 km for σ_w^2, about 9.5 km for σ_{turb}^2, and about 7.5 km for C_n^2. The relatively lower height for the maximum of C_n^2 is likely due to the influence of humidity advected upward during convection on the mean gradient of the refractive index.
4) The probability density distributions of C_n^2 and σ_{turb}^2 near their levels of maximum enhancement are unimodal, with the modes steadily increasing with increasing proximity of convection. However, the probability density distribution of σ_w^2 is bimodal in all instances, suggesting that there can be enhanced wave activity even when visible convection is not present and that the presence of a thunderstorm at the station does not necessarily indicate greatly enhanced wave activity.
5) Zonal wind speeds are relatively light and vertical wind shear is small at all heights during convection cases in comparison with no-convection cases.

Acknowledgments. This study was supported in part by the Air Force Office of Scientific Research.

REFERENCES

Alexander, M. J., J. R. Holton, and D. J. Durran, 1995: The gravity wave response above deep convection in a squall line simulation. *J. Atmos. Sci.,* **52,** 2212–2226.

Bowhill, S., and S. Gnanalingam, 1986: Gravity waves in severe weather. *Proc. Third Workshop on Technical and Scientific Aspects of MST Radar,* Aguadilla, Puerto Rico (Handbook for MAP, Vol. 20), SCOSTEP, 128–135.

Chun, H.-Y., M.-D. Song, and J.-W. Kim, 2001: Effects of gravity wave drag induced by cumulus convection on the atmospheric general circulation. *J. Atmos. Sci.,* **58,** 302–319.

Dewan, E. M., and Coauthors, 1998: MSX satellite observations of thunderstorm-generated gravity waves in midwave infrared images of the upper stratosphere. *Geophys. Res. Lett.,* **25,** 939–942.

Ecklund, W. L., K. S. Gage, and B. B. Balsley, 1981: A comparison of vertical wind variability observed with the Platteville VHF radar and local weather conditions. Preprints, *20th Conf. on Radar Meteorology,* Boston, MA, Amer. Meteor. Soc., 104–108.

Fritts, D. C., and G. D. Nastrom, 1992: Sources of mesoscale variability of gravity waves. Part II: Frontal, convective, and jet stream excitation. *J. Atmos. Sci.,* **49,** 111–127.

Gage, K. S., 1990: Radar observations of the free atmosphere: Structure and dynamics. *Radar in Meteorology,* D. Atlas, Ed., Amer. Meteor. Soc., 534–565.

Gossard, E. E., and W. H. Hooke, 1975: *Waves in the Atmosphere.* Elsevier, 456 pp.

Green, J. L., R. H. Winkler, J. M. Warnock, W. L. Clark, K. S. Gage, and T. E. VanZandt, 1978: Observations of enhanced clear air reflectivity associated with convective clouds. Preprints, *18th*

Conf. on Radar Meteorology, Atlanta, GA, Amer. Meteor. Soc., 88–93.

Hansen, A. R., G. D. Nastrom, and F. D. Eaton, 2001: Seasonal variation of gravity wave activity at 5–20 km observed with the VHF radar at White Sands Missile Range, New Mexico. *J. Geophys. Res.,* **106,** 17 171–17 183.

Lane, T. P., and M. J. Reeder, 2001: Modeling the generation of gravity waves by a maritime continent thunderstorm. *Quart. J. Roy. Meteor. Soc.,* **127,** 2705–2724.

——, ——, and T. L. Clark, 2001: Numerical modeling of gravity wave generation by deep tropical convection. *J. Atmos. Sci.,* **58,** 1249–1274.

Larsen, M. F., W. E. Swartz, and R. F. Woodman, 1982: Gravity-wave generation by thunderstorms observed with a vertically-pointing 430 MHz radar. *Geophys. Res. Lett.,* **9,** 571–574.

Lu, D., T. E. VanZandt, and W. L. Clark, 1984: VHF Doppler radar observations of buoyancy waves associated with thunderstorms. *J. Atmos. Sci.,* **41,** 272–282.

McLandress, C., M. J. Alexander, and D. L. Wu, 2000: Microwave Limb Sounder observations of gravity waves in the stratosphere: A climatology and interpretation. *J. Geophys. Res.,* **105,** 11 947–11 967.

Nastrom, G. D., and K. S. Gage, 1984: A brief climatology of vertical wind variability in the troposphere and stratosphere as seen by the Poker Flat, Alaska MST radar. *J. Climate Appl. Meteor.,* **23,** 453–460.

——, and F. D. Eaton, 1993: The coupling of gravity waves and turbulence at White Sands, New Mexico, from VHF radar observations. *J. Appl. Meteor.,* **32,** 81–87.

——, and ——, 1995: Variations of winds and turbulence seen by the 50-MHz radar at White Sands Missile Range, New Mexico. *J. Appl. Meteor.,* **34,** 2135–2148.

——, and ——, 1997: Turbulence eddy dissipation rates from radar observations at 5–20 km at White Sands Missile Range, New Mexico. *J. Geophys. Res.,* **102,** 19 495–19 506.

Pandya, R. E., and M. J. Alexander, 1999: Linear stratospheric gravity waves above convective thermal forcing. *J. Atmos. Sci.,* **56,** 2434–2446.

Petitdidier, M., P. B. Chilson, and C. W. Ulbrich, 1997: Observations of gravity waves and turbulence associated with a tropical thunderstorm. *Proc. 1st SPARC General Assembly,* Melbourne, Australia, WMO/TD-814, 401–404.

Roettger, J., 1980: Structure and dynamics of the stratosphere and mesosphere revealed by VHF radar investigations. *Pure Appl. Geophys.,* **118,** 496–527.

Rosenblatt, M., 1956: Remarks on some nonparametric estimates of a density function. *Ann. Math. Stat.,* **27,** 832–837.

Rüster, R., G. D. Nastrom, and G. Schmidt, 1998: High-resolution VHF radar measurements in the troposphere with a vertically pointing beam. *J. Appl. Meteor.,* **37,** 1522–1529.

Sato, K., 1992: Vertical wind disturbances in the afternoon of midsummer revealed by the MU radar. *Geophys. Res. Lett.,* **19,** 1943–1946.

——, 1993: Small-scale wind disturbances observed by the MU radar during the passage of Typhoon Kelly. *J. Atmos. Sci.,* **50,** 518–537.

——, H. Hashiguchi, and S. Fukao, 1995: Gravity waves and turbulence associated with cumulus convection observed with the UHF/VHF clear-air Doppler radars. *J. Geophys. Res.,* **100,** 7111–7119.

Tsuda, T., Y. Murayama, H. Wiryosumarto, S. W. B. Harijono, and S. Kato, 1994: Radiosonde observations of equatorial atmospheric dynamics over Indonesia. 2. Characteristics of gravity waves. *J. Geophys. Res.,* **99,** 10 507–10 516.

Vincent, R. A., and M. J. Alexander, 2000: Gravity waves in the tropical lower stratosphere: An observational study of seasonal and interannual variability. *J. Geophys. Res.,* **105,** 17 971–17 982.

Weinstock, J., 1981: Energy dissipation rates of turbulence in the stable free atmosphere. *J. Atmos. Sci.,* **38,** 880–883.

Whiteway, J. A., 1999: Enhanced and inhibited gravity wave spectra. *J. Atmos. Sci.,* **56,** 1344–1352.

Yang, M.-J., and R. A. Houze Jr., 1995: Multicell squall-line structure as a manifestation of vertically trapped gravity waves. *Mon. Wea. Rev.,* **123,** 641–661.